scientific reports

Check for updates

OPEN

Exchange bias effect in polycrystalline $Bi_{0.5}Sr_{0.5}Fe_{0.5}Cr_{0.5}O_3$ bulk

S. Z. Li[1]✉, A. Rahman[2], C. L. Ma[3], X. Zhao[1], Z. Y. Sun[1], M. F. Liu[4], X. Z. Wang[4], X. F. Xu[5] & J. M. Liu[6]

Bulk $Bi_{0.5}Sr_{0.5}Fe_{0.5}Cr_{0.5}O_3$ (BSFCO) is a new compound comprising the *R3c* structure. The structural, magnetic property and exchange bias (EB) details are investigated. The material was in the super-paramagnetic (SP) state at room temperature. Exchange bias usually occurs at the boundary between different magnetic states after field cooling (H_{FC}) acts on the sample. Here the result shows that changing H_{FC} from 1 to 6 T reduces the H_{EB} value by 16% at 2 K at the same time. Meanwhile, H_{EB} diminishes as the ferromagnetic layer thickness increases. The variation of (the thickness of ferromagnetic layer) t_{FM} with the change of H_{FC} leads to the tuning of H_{EB} by H_{FC} in BSFCO bulk. These effects are obviously different from the phenomenon seen in other oxide types.

Exchange coupling often occurs at the interface between the ferromagnetic (FM) and antiferromagnetic (AF) layers. When a magnetic field *(H)* is applied, once the sample temperature is below the AF layer Néel temperature, the FM layer exhibits unidirectional anisotropy because of the exchange coupling[1,2]. As a result, the hysteresis loop shifts along the field axis. The strength of the shift is called by the exchange bias (EB). The EB effect is attributed to a FM unidirectional anisotropy formed at the interface between different magnetic phased[3]. There are some EB effects in artificial material systems, for example, FM-AFM bilayers, FM-AFM superlattices, and topological-insulator/antiferromagnet containing ferromagnetic antiferromagnetic (FM-AFM) components[4–11].

Up to now, some progress has been made in the investigation of man-made EB structures. However, there are still some issues with the use of artificial structures that have been modified with various material phases. The artificial EB usually benefits from field-cooling process. But artificial material with chaotic ionic diffusion at the interface maybe influences on the FM-AFM coupling. In recent years, investigations have demonstrated unusual EB under field-cooling (FC) and large spontaneous EB in a variety of systems with a single phase, including $BiFeO_3$–$Bi_2Fe_4O_9$ nanocomposite, NiMnIn, Mn_2PtGa, $La_{1.5}Sr_{0.5}MnCoO_6$, $Pb_6Ni_9(TeO_6)_5$, $Y_{0.2}Ca_{0.8}MnO_3$, and $Bi_{10}Fe_6Ti_3O_{30}$ polycrystalline samples[6,12–17].

From above, materials with EB effect in a single phase should be investigated further to better understand the mechanism. Baettig and Spaldin performed first-principles calculations on the $BiFeO_3$–$BiCrO_3$ system[18]. A double-perovskite Bi_2FeCrO_6 with a long-range Fe^{3+}–Cr^{3+} order was hypothetically constructed, and a magnetic moment of 2 μB per formula unit were predicted [18]. Experiments focused on the substituting effect of Cr ion for Fe ion on the physical properties of BFO[19]. But in bulk, it is difficult to prepare, so $SrCrO_3$ and $Bi(Fe,Cr)O_3$ must be both prepared under high pressure[20]. For BFO, $Bi(Fe,Cr)O_3$ and $SrCrO_3$ bulk, appearance of weak FM could result in glassy state between AFM and FM interactions. Therefore, we investigate the $Bi_{0.5}Sr_{0.5}Fe_{0.5}Cr_{0.5}O_3$ system in search of stable perovskite phases that may exhibit some of the above properties. Here the structure and magnetic properties of the new phase $Bi_{0.5}Sr_{0.5}Fe_{0.5}Cr_{0.5}O_3$ under ambient pressure. And we present the observation FM, AFM and SP in the BSFCO bulk and discuss the role of multiple of magnetic phases on EB effects. The results show that $Bi_{0.5}Sr_{0.5}Fe_{0.5}Cr_{0.5}O_3$ bulk has the potential to be a new class material, which could help to improve magnetic tuning.

[1]School of Electrical and Electronic Engineering, Wuhan Polytechnic University, Wuhan 430048, China. [2]Department of Physics, University of Science and Technology of China, Hefei 230026, China. [3]Jiangsu Key Laboratory of Micro and Nano Heat Fluid Flow Technology and Energy Application, School of Physical Science and Technology, Suzhou University of Science and Technology, Suzhou 215009, China. [4]Institute for Advanced Materials, Hubei Normal University, Huangshi 435002, China. [5]Institution of Quatum Material, Hubei Polytechnic University, Huangshi 435003, China. [6]Nanjing National Laboratory of Microstructure, Nanjing University, Nanjing 210093, China. ✉email: origen2003@126.com

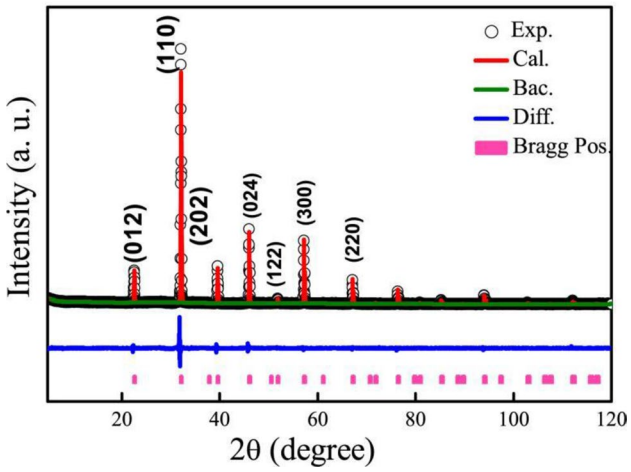

Figure 1. X-ray diffraction patterns for BSFCO are shown at the room temperature. The refined structure diffraction data are observed together with the experimental data points using Gasa refinement.

Experiments

$Bi_{0.5}Sr_{0.5}Fe_{0.5}Cr_{0.5}O_3$ (BSFCO) bulk was prepared by solid reaction. High-purity $SrCO_3$, Bi_2O_3 (10% excess), Fe_2O_3, and Cr_2O_3 were intimately synthesized for 24 h, in stoichiometric quantities with solid reaction method under flowing nitrogen at 950 °C and 1100 °C. X-ray powder diffraction supplied the formation of a single perovskite type phase. Measurements of the crystal structure of the samples were performed on a 'Rigaku UltimaIV' X-ray diffraction apparatus (XRD, 285 mm 3 kW and CuKα1). The data were analyzed by using the GSAS suite of Rietveld analysis programs. A superconducting quantum interference device magnetometer (SQUID, Quantum Design Inc.) was employed to carry out magnetization measurements. After undergoing zero field cooling (ZFC) and field cooling (FC), measurements were conducted when the sample was heated from 5 to 300 K under $H = 10$ kOe. A magnetization loop was measured at 2 K. Mössbauer data were obtained using a conventional constant acceleration Mössbauer spectrometer incorporating a 25 mCi source of ^{57}Co in an Rh matrix. The valence states of Fe ions and Cr ions in bulk BSFCO were detected by the X-ray photoelectron spectroscopy (Al kα source, $h\nu = 1.486$ eV).

Results

XRD patterns. Figure 1 depicts the XRD patterns of $Bi_{0.5}Sr_{0.5}Fe_{0.5}Cr_{0.5}O_3$ at room temperature. The diffraction data reveals the same structure with a hexagonal *R3c* unit cell, which is similar with $BiFeO_3$ previously reported[20]. Since Sr ionic has a smaller size than that of Ba ion and the ionic size of Cr is smaller than that of Fe, this leads to the lattice constants change. To discuss the crystal lattice structure changes, the structure was refined using Rietveld, and the data was fitted to the experimental pattern. The lattice parameters were refined and shown with $Chi^2 = 1.877$, $R_{wp} = 5.97\%$, $R_p = 4.58\%$ in Table 1. The cell parameters of sample were $a = 5.5726(22)$ Å, $b = 5.5726(22)$ Å, $c = 13.6500(64)$ Å. The site of the cell is *x*, *y* and *z* in Table 1. It is found that the lattice constant that *a* and *c* decrease because Sr and Cr substitute Bi and Fe, respectively. The in-plane lattice parameter *a* is reduced to 5.572 Å, and the out-of-plane lattice parameter *c* decreases and is up to 13.6500 Å. No additional reflections and impurities are detected in the room-temperature XRD data of bulk $Bi_{0.5}Sr_{0.5}Fe_{0.5}Cr_{0.5}O_3$.

In order to get the atomic valence, Fig. 2 illustrates the Fe 2p and Cr 2p XPS spectra of bulk $Bi_{0.5}Sr_{0.5}Fe_{0.5}Cr_{0.5}O_3$. Figure 2a shows the binding energies of Cr 2p. The energies 576.2 eV and 586.2 eV correspond to Cr $2p_{3/2}$ and Cr $2p_{1/2}$, respectively. It demonstrates that the Cr ions in BSFCO are mainly Cr^{3+}[22]. The Fe $2p_{3/2}$ and Fe $2p_{1/2}$ peaks are at about 711.7 eV and 725.3 eV in Fig. 2b, respectively. Fe^{3+} ions have binding energies. And Fe $2p_{1/2}$ with a satellite is at 719.6 eV[21,22]. Therefore, it can be deduced that Fe ions in the bulk BSFCO are primarily Fe^{3+}, with a few Fe^{2+} ions present to compensate for oxygen vacancies that cannot be determined.

Atom (site)	*x*	*y*	*z*	Occ	U_{iso}
Bi1(6*a*)	0.0000	0.0000	− 0.1668(2)	0.5000	0.0866(8)
Fe1(6*a*)	0.0000	0.0000	0.0838(3)	0.5000	0.0195(9)
Sr1(6*a*)	0.0000	0.0000	− 0.1668(2)	0.5000	0.0866(8)
Cr1(6*a*)	0.0000	0.0000	0.0838(3)	0.5000	0.0195(9)
O1(18*b*)	0.5038(2)	0.5001(1)	0.8383(5)	1.0000	0.0363(5)

Table 1. Refined structural parameters of $Bi_{0.5}Sr_{0.5}Fe_{0.5}Cr_{0.5}O_3$ from powder diffraction data collected at room temperature. SP: *R3c*, $a = 5.5726(22)$ Å, $b = 5.5726(22)$ Å, $c = 13.6500(64)$ Å, $Chi^2 = 1.877$, $R_{wp} = 5.97\%$, $R_p = 4.58\%$.

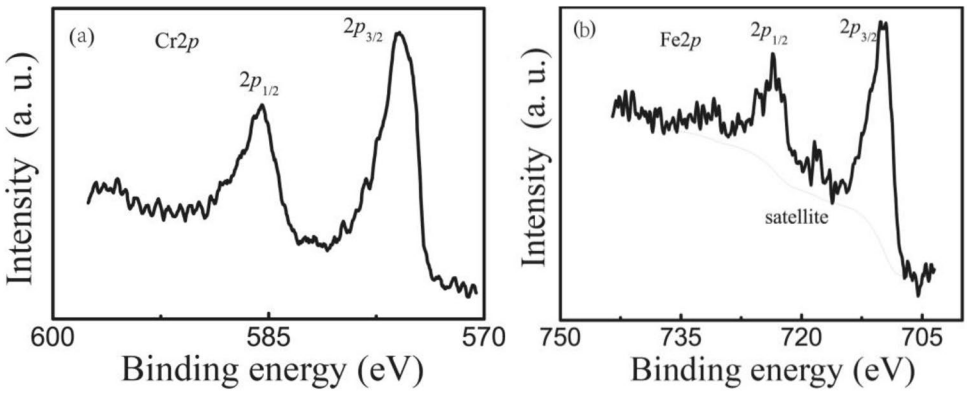

Figure 2. The core level XPS spectra for constituent elements in bulk BSCFO (**a**) $Cr^{3+}$and (**b**) for Fe^{3+}.

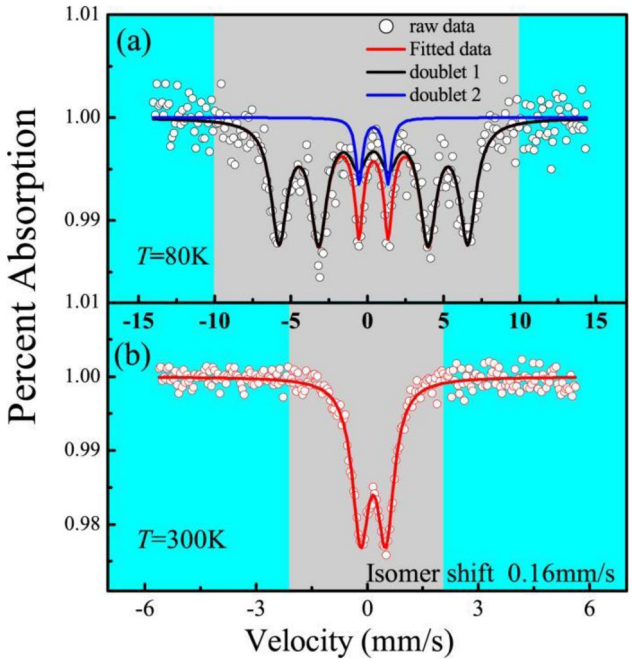

Figure 3. The Mössbauer data of bulk BSCFO at 80 K (**a**) and 300 K (**b**).

The Mössbauer spectrum and magnetization of bulk BSFCO. Mössbauer data for bulk BSFCO samples at 80 K (a) and 300 K (b) are shown in Fig. 3. Mössbauer spectroscopy is used to demonstrate the bulk magnetic behavior. The 80-K spectrum in Fig. 3a was fitted to a six-line magnetic profile (doublet 1 in black, $Chi^2 = 1.2$) and a double magnetic profile (doublet 2 in blue, $Chi^2 = 0.9$). In Fig. 3b, the data can be fitted to a doublet profile and shows super-paramagnetic relaxation at 300 K. All related data are shown in Table 2. At 300 K, it is a paramagnetic/antiferromagnetic material with an isomer shift of 0.16(0) mm/s. The property of quadrupole splitting indicates the presence of a distorted octahedral environment, which agrees with bond distances refined from X-ray diffraction.

As the temperature decreases, there are strong super-exchange interactions between the metal ions, which causes the splitting of the magnetic energy levels of the nuclei, thus making the Mössbauer spectrum exhibit a magnetic splitting six-line magnetic profile and super-paramagnetic relaxation. In Fig. 3a, the quadrupole interaction at 80 K is 0.40(7) mm/s, which is the characteristc of Fe^{3+}[23]. Meanwhile, the width of the spectrum at 80 K is wider than that at 300 K. The areas of doublet 1 and doublet 2 are 90.9% and 9.1% with super-magnetic relaxation, respectively. The ferromagnetic component of the spectrum becomes stronger and the paramagnetic component becomes weaker. Therefore, the paramagnetic spectrum in the sample spectra should be derived from the super-paramagnetic relaxation caused by the small size effect[24].

ZFC-Field cooling (FC) curves are measured to investigate the magnetization of bulk BSFCO at low temperatures as shown in Fig. 4. And enlarged ZFC curve is in the inset. Figure 4 shows the magnetization curves of

Temperature	*Area*	*IS** (mm/s)	*QS* (mm/s)	*H (kOe)*	*W* Γ (mm/s)
300 K		0.16(0)	0.67(8)		0.54(6)
80 K	90.9%	0.40(7)		383.(3)	1.28(4)
	9.1%	0.41(7)	1.89(2)		0.54(0)

Table 2. Mössbauer data at 300 K and 80 K for BSFCO bulk.

bulk BSFCO at zero field and cooling field after $H = 10$ kOe and $T = 300$ K. The bulk magnetic behavior of BSFCO is revealed by magnetization measurements and plotted as a *M-T* curve. The ZFC curve has a plate-like peak at 25 K and the magnetization decreases rapidly below 25 K, while the ZFC and FC curves split around 130 K, which is similar to that of Ni-Mn-In bulk alloys[13]. It is an obvious feature of coexisting FM (super-ferromagnetic) cluster and an AFM matrix. The super-ferromagnetic domains are collectively frozen forming spin glass (SG) state at lower temperatures.[13]The plate-like curve suggests the existence of competing interactions among its ferromagnetic property, antiferromagnetic property and SG. Consequently, it may not be linked to spin glass-like freezing with long range order, but a transition to short range order.

***M–H* properties.** To confirm these magnetic properties, the hysteresis loops of magnetization were collected from – 10 kOe to 10 kOe at 2 K after ZFC; And the data were gotten from FC under $H = 10$ kOe decreasing from 300 K, as shown in Fig. 5. The *M–H* loop under ZFC state is symmetric around zero, whereas the existence of exchange bias was proved by the shift of FC loops towards negative field. H_{EB} and H_C parameters are defined as $H_{EB} = (H_1 + H_2)/2$ and $H_C = -(H_1 - H_2)/2$, respectively, where H_1 and H_2 are the left and right coercivity field. H_{EB} was about 1150 Oe under the FC condition. H_C obtained from the FC loop is about 460 Oe and it is slightly higher than H_C obtained from ZFC (410 Oe). The different values result from the function of the exchange anisotropy because the magnetic field acts or not.

It is shown in Fig. 6, with the reduction of H_{EB} and H_C by the reversal of subsequent magnetization, the so-called training effect is present. This effect indicates that the exchange anisotropy slowly decreases. From the *M-H* loops (Fig. 6), it is observed that the ZFC magnetizations at 10 kOe, 35 kOe, and 50 kOe are much smaller than that of their FC counterparts. So FC can enlarge the content of the super-ferromagnetic (SFM) or FM region and ferromagnetic layer (t_{FM}). The increase of t_{FM} under FC conditions reduces strain anisotropy, which arises from different magnetic states among the FM layer, the AF layer, and disordered spin glass; meanwhile, the strain anisotropy could cause the decrease of H_C.

From above, we can deduce that changing H_{FC} can affect t_{FM} and the ratio of H_C (H_c under FC) and H_{EB} (H_{EB} under FC), as shown in Fig. 7. When H_{FC} increases, both H_C and H_{EB} decrease. When H_{FC} increases from 10 to 60 kOe, H_{EB} decreases by 16% at 2 K. It is not difficult to conclude from the above analysis that strain anisotropy could decrease[16]. When the sample under FC exists, an FM-AFM interface with unidirectional FM spins formed. On one hand, it is known that AFM domains with anisotropy axis parallel to external magnetic. On the other hand, for AFM domains with anisotropy axis nonparallel to external magnetic field, there is an angle between the direction of the initial magnetization. So increasing external magnetic field, H_{EB} will decrease[10].

To demonstrate the relationship between t_{FM} and H_{EB} in bulk BSCFO, the dependence of t_{FM} on H_{FC} must be confirmed. From the *M-H* loop in Fig. 6, the magnetization of the FM layers is almost observed under an applied field of 10 kOe. M_{sat}, defined as $(M_{10kOe}\text{-}M_{\text{-}10kOe})/2$, is proportional to the volume fraction of the FM region[3]. M_{sat} increases with H_{FC} when t_{FM} emerges, so the M_{sat}-H_{FC} curve in Fig. 8 scales the variation of t_{FM} with H_{FC}. H_{EB} and $1/M_{sat}$ have a quasi-linear relationship, as illustrated in Fig. 8. H_{EB} decreases as t_{FM} increases, which is consistent with the trend in exchange bias films[3]. The result demonstrates the presence of FM coupling at the FM/AF interface in BSCFO. In the further, the AF coupling at the interface would result in a competition between the exchange energy and the Zeeman energy. It would weaken the relationship between H_{EB} and $1/t_{FM}$. This trend deviates from the linear prediction. It is worth noting that H_{FC} changes the anti-ferromagnetic thickness (t_{AF}), which has an impact on H_{EB}.

This implies that the majority of the regions in the system are AF, but t_{FM} remains constant after sample fabrication without being affected by H_{FC}. The interfacial spins of SFM and/or AF layers with H_{FC} will have an effect on H_{EB} change. The spontaneous FM and AF layers in BSCFO remain constant, allowing t_{FM} to be tuned after fabrication utilizing external forces. The mutual interactions of charge, defects, spin, and lattice degrees of freedom in this bulk material can result in a delicate balance of different ground states[3,10].

In order to explore the above phenomenon, the evolution of the SFM/AFM spin interface of BSFCO after FC under external magnetic field was shown in Fig. 9. It is a simplified schematic diagram with SFM or FM/AFM interface embedded in an AFM domain. Wang et. al. believe that a SFM unidirectional anisotropy, which is similar to an FM unidirectional anisotropy, can be formed during the initial magnetization process[13].The applied magnetic field aligns some of the AFM spin along the direction of external field. FM structure can be influenced with AFM by interfacial coupling, so the magnetization can be changed to a greater extent under a PM background, as shown in Fig. 9 (①②③). Because the Zeman energy of AFM spins near the interface is larger than the coupling energy of AFM/FM at the interface. Some AFM spins can aligned along the direction of external field. It is identified from above that external fields have an effect on the interaction between the AF and FM layers in Fig. 9(②③). Furthermore, it benefits FM phase enhancement, as increasing H_{FC} can increase the ration of FM content and t_{FM} while decreasing H_{EB}. This indicates that, in the presence of certain external factors, the sensitivities of order parameters can be used to tune the exchange bias. Some recent studies suggest

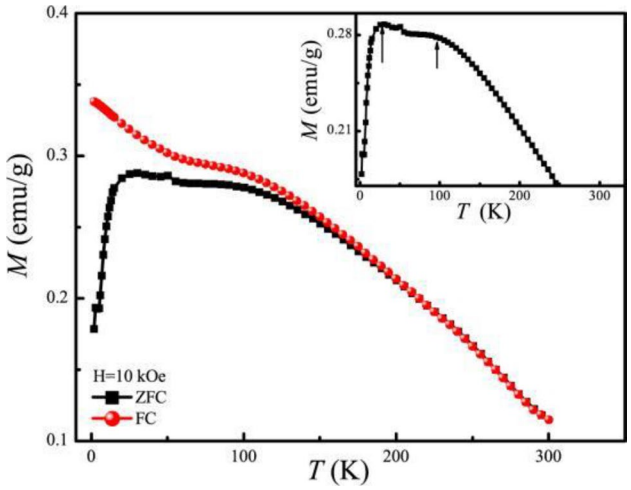

Figure 4. The ZFC and FC curve of BSCFO bulk under $H = 10$ kOe.

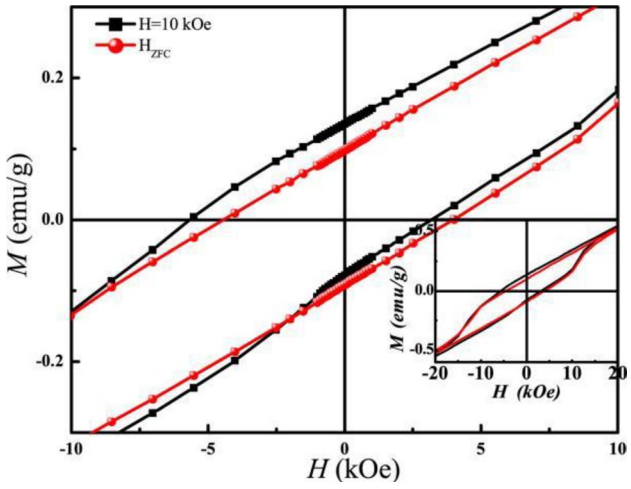

Figure 5. Hysteresis loops of magnetization at 2 K after ZFC and FC under $H = 10$ kOe from 300 K. The inset is the enlarged graph of hysteresis loop.

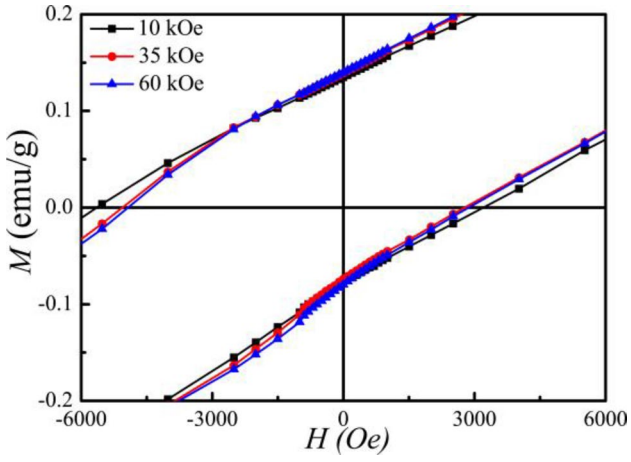

Figure 6. Hysteresis loops of magnetization at 2 K after FC under $H = 10$ kOe, 35 kOe and 60 kOe.

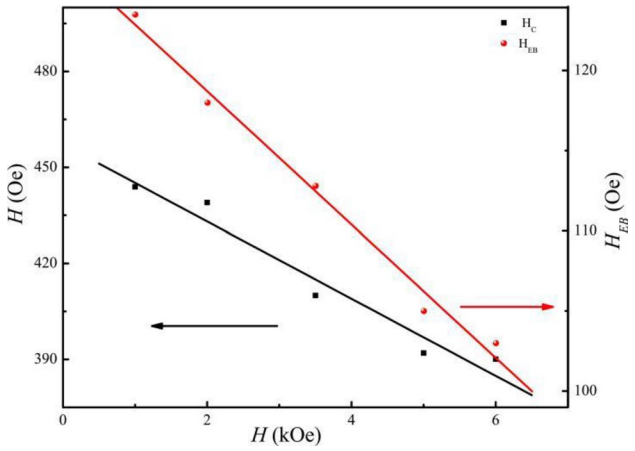

Figure 7. H_{FC} dependence of H_C (right-hand axis) and H_{EB} (left-hand axis) at 2 K. H_C and H_{EB} decrease linearly with H_{FC}. The lines are provided as a guide to the eye.

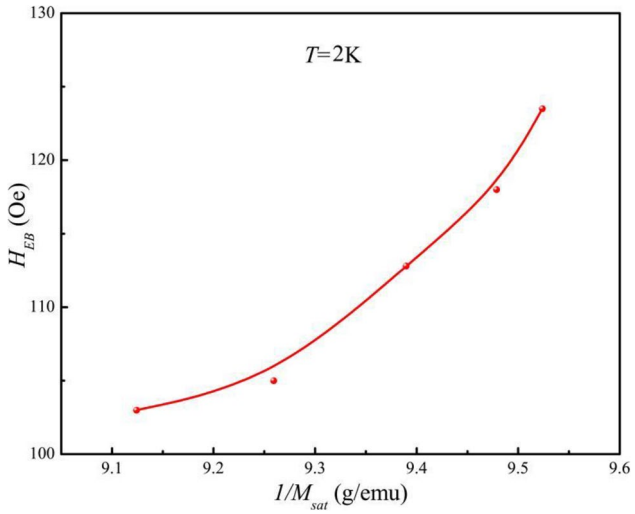

Figure 8. Linear relationship between H_{EB} and $1/M_{sat}$ at 2 K. Note that M_{sat} scales t_{FM}, indicating that the exchange bias in bulk BSFCO follows $H_{EB} \propto 1/t_{FM}$.

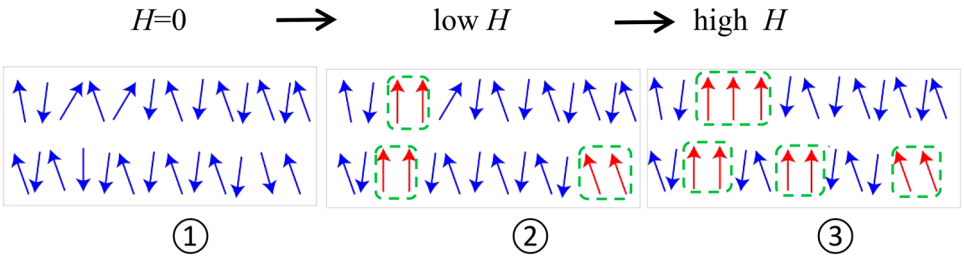

Figure 9. Schematic diagram of the AFM/FM structure for bulk BSCFO under different magnetic fields. The datasets generated and/or analyzed during the current study are available in the [CSD Crystallographic data] repository, [Summary of Data—Deposition Number 2151932, Compound Name:Data Block Name: data_ BFSC_publ Unit Cell Parameters: a 5.57262(5) b 5.57262 c 13.65006(10) R3c.

that short disorder is beneficial to FM clusters/microstructure in $La_{1.5}Sr_{0.5}CoMnO_6$ and Mn_2PtGa materials[6,13]. The exchange anisotropic coupling of the embedded phase between FM and AFM layers has resulted in EB. Thus, it's reasonable to assume that the EB in bulk BSFCO is due to the coupling between the AFM layer and SFM or

FM layer. To summarize, the analysis of exchange bias in these types of materials may lead to unusual events, which could aid in the creation of multifunctional spintronic devices.

Data availability

All data generated or analysed during this study are included in this published article and supplementary files.

Received: 7 January 2022; Accepted: 31 March 2023
Published online: 18 April 2023

References

1. Soumyanarayanan, A. *et al.* Tunable room-temperature magnetic skyrmions in Ir/Fe/Co/Pt multilayers. *Nat. Mater.* **16**, 898–904 (2017).
2. Skumryev, V. *et al.* Beating the superparamagnetic limit with exchange bias. *Nature (London)* **423**, 850–853 (2003).
3. Nogués, J. & Schuller, I. K. Exchange bias. *J. Magn. Magn. Mater.* **192**, 203–232 (1999).
4. Rodríguez-Suárez, R. L. *et al.* Tunable misalignment of ferromagnetic and antiferromagnetic easy axes in exchange biased bilayers. *Appl. Phys. Lett.* **100**, 242406–4 (2012).
5. Maity, T., Goswami, S., Bhattacharya, D. & Roy, S. Superspin, glass mediated giant spontaneous exchange bias in a nanocomposite of $BiFeO_3$-$Bi_2Fe_4O_9$. *Phys. Rev. Lett.* **110**, 107201–2 (2013).
6. Nayak, A. K. *et al.* Large zero-field cooled exchange-bias in bulk Mn_2PtGa. *Phys. Rev. Lett.* **110**(127204), 1–4 (2013).
7. Kanazawa, N. *et al.* Large topological hall effect in a short-period helimagnet MnGe. *Phys. Rev. Lett.* **106**(156603), 1–4 (2011).
8. Dong, S., Zhang, Q. F., Yunoki, S. J., Liu, J.-M. & Dagotto, E. Magnetic and orbital order in $(RMnO_3)_n/(AMnO_3)_{2n}$ superlattices studied via a double-exchange model with strain. *Phys. Rev. B* **86**, 205121 (2012).
9. Ye, M. *et al.* Carrier-mediated ferromagnetism in the magnetic topological insulator Cr-doped (Sb, Bi)$2T_e3$. *Nat. Commun.* **6**(8913), 1–8 (2015).
10. Nogue's, J., Moran, T. J., Lederman, D., Schuller, I. K. & Rao, K. V. Role of interfacial structure on exchange-biased FeF_2-Fe. *Phys. Rev. B* **19**, 6984 (1999).
11. Gruyters, M. Spin-glass-like behavior in CoO nanoparticles and the origin of exchange bias in layered CoO ferromagnet structures. *Phys. Rev. Lett.* **95**(077204), 1–4 (2005).
12. Maity, T., Goswami, S., Bhattacharya, D. & Roy, S. Superspin, glass mediated giant spontaneous exchange bias in a nanocomposite of $LiFeO_3$–$Bi_2Fe_4O_9$. *Phys. Rev. Lett.* **110**, 107201 (2013).
13. Wang, B. M. *et al.* Large exchange bias after zero-field cooling from an unmagnetized state. *Phys. Rev. Lett.* **106**(077203), 1–4 (2011).
14. Murthy, J. K. & Venimadhav, A. Giant zero feld cooled spontaneous exchange bias effect in phase separated $La_{1.5}Sr_{0.5}CoMnO_6$. *Appl. Phys. Lett.* **103**, 252410 (2013).
15. Koteswararao, B. *et al.* Large spontaneous exchange bias in a weak ferromagnet $Pb_6Ni_9(TeO6)_5$. *Sci. Rep.* **5**(16480), 1–7 (2017).
16. Qian, T. *et al.* Exchange bias tuned by cooling field in phase separated $Y_{0.2}Ca_{0.8}MnO_3$. *Appl. Phys. Lett.* **90**, 012503 (2007).
17. Huang, Y. *et al.* Observation of exchange anisotropy in single-phase layer-structured oxides with long periods. *Sci. Rep.* **5**(15261), 1–10 (2015).
18. Baettig, P., Ederer, C. & Spaldin, N. A. First principles study of the multiferroics $BiFeO_3$, Bi_2FeCrO_6, and $BiCrO_3$: Structure, polarization, and magnetic ordering temperature. *Phys. Rev. B* **72**(214105), 1–8 (2005).
19. Kim, D. H., Lee, H. N., Varela, M. & Christen, H. M. Antiferroelectricity in multiferroic $BiCrO_3$ epitaxial films. *Appl. Phys. Lett.* **89**(162904), 1–3 (2006).
20. Ortega-San-Martin, L., Williams, A. J., Storer, A. & Attfifield, J. P. Frustrated orders in the perovskite $(Bi_{0.5}Sr_{0.5})CrO_3$. *Chem. Mater.* **21**, 2436–2441 (2009).
21. Mills, P. & Sullivan, J. L. A study of the core level electrons in iron and its three oxides by means of X-ray photoelectron spectroscopy. *J. Phys. D* **16**, 723–732 (1983).
22. Moudler, J. F., Stickle, W. F., Sobol, P. E. & Bomben, K. D. *Handbook of X-ray Photoelectron Spectroscopy* 77–81 (Perkin-Elmer, Eden Prairie, 1992).
23. Suchomel, M. R., Thomas, C. I., Allix, M., Rosseinsky, M. J. & Fogg, A. M. High pressure bulk synthesis and characterization of the predicted multiferroic $Bi(Fe_{1/2}Cr_{1/2})O_3$. *Appl. Phys. Lett.* **90**(112909), 1–4 (2007).
24. Jiang, H. *et al.* Bio-derived hierarchical multicore-shell Fe_2N-nanoparticle-impregnated N-doped carbon nanofber bundles: a host material for lithium-potassium-ion storage. *Nano-Micro Lett.* **11**(56), 1–17 (2019).

Acknowledgements

Research was sponsored by the National Natural Science Foundation of China (11374147, 12074111);Science and Technology Support Action Plan of 'Universities serve rural revitalization' by Hubei Provincial Department of Education(No. BXLBX0497).

Author contributions

S.L., A.R., C.L.M., X.Z., Z Y.S., M F.L. wrote the main manuscript text; M.F.L. prepared figures. All authors reviewed the manuscript.

Competing interests

The authors declare no competing interests.

Additional information

Supplementary Information The online version contains supplementary material available at https://doi.org/10.1038/s41598-023-32734-x.

Correspondence and requests for materials should be addressed to S.Z.L.

Reprints and permissions information is available at www.nature.com/reprints.

Publisher's note Springer Nature remains neutral with regard to jurisdictional claims in published maps and institutional affiliations.